PHYSICAL REVIEW E, VOLUME 63, 065302(R)

Method for measuring local hydraulic permeability using magnetic resonance imaging

Martin Bencsik* and Chandrasekhar Ramanathan
Magnetic Resonance Centre, School of Physics and Astronomy, University of Nottingham, University Park, Nottingham NG7 2RD, England

(Received 19 December 2000; published 24 May 2001)

The hydraulic permeability of a porous medium characterizes the ease with which a fluid may be driven through it, and is defined via the classical Darcy law. A method for noninvasive, nondestructive measurement of one projection of the local permeability tensor of a porous medium, using gas phase magnetic resonance imaging, is presented. Results are shown for one-dimensional experiments on dry porous rocks. The limitations of the method are explored, and the extension to three-dimensional imaging of the permeability is discussed.

DOI: 10.1103/PhysRevE.63.065302 PACS number(s): 47.55.Mh, 76.60.Pc, 81.05.Rm

INTRODUCTION

The permeability of a medium represents the ease with which a fluid may be driven through it, and is a characteristic of the medium only. It is a critical parameter in the modeling of fluid transport in a wide range of applications from oil-well reservoir engineering to the drying of cements. The measurement of local permeabilities remains a challenging problem. Currently, the direct measurement of local variations in permeability is only possible by placing pressure sensors inside the medium, or alternatively, the material can be physically sectioned and the permeability of each individual element measured. Indirect estimates of permeability can be obtained from tortuosity measurements using electrical conductivity experiments. It has recently been shown that such tortuosity measurements can also be made directly with gas phase NMR [1]. NMR estimates of permeability have also been obtained indirectly from measurement of the porosity of the material and the pore surface to volume ratio using NMR relaxation times [2–7], as well as from NMR diffusion measurements [8,9]. This paper presents a noninvasive method to *directly* measure the permeability of a porous medium.

For a Newtonian fluid, laminar flow through a porous medium can be described by the differential form of Darcy's law [10];

$$\mathbf{q}(\mathbf{r}) = -\frac{\underline{\kappa}(\mathbf{r})}{\eta(\mathbf{r})}\nabla P(\mathbf{r}), \tag{1}$$

where $P(\mathbf{r})$ is the local pressure, $\mathbf{q}(\mathbf{r})$ the local fluid flow vector, $\underline{\kappa}(\mathbf{r})$ the local permeability tensor, and $\eta(\mathbf{r})$ the local fluid viscosity. This law holds on mesoscopic or larger scales. If the fluid flowing through a porous material is compressible, then the local pressure will be related to its density. In an NMR experiment on such a system, the nuclear magnetization is proportional to the density of spins and therefore to pressure. The resulting NMR signal is also proportional to the spin density, to first order. It is thus possible to obtain an image of the local pressure distribution in the medium. This measurement can then be used to derive the pressure gradient in Eq. (1), and permits the determination of the medium permeability as shown below.

Consider the one-dimensional (1D) situation of a gas flowing through a porous medium, as shown in Fig. 1. If a pressure drop measurement is made along the direction of the main flow **Q**, the total fluid volume flow rate at position z, $q(z)$ is related to the local permeability and local pressure gradient by the projection of Eq. (1) along the z direction,

$$q(z) = -\frac{\kappa(z)}{\eta(z)}\frac{dP(z)}{dz}. \tag{2}$$

Under steady-state flow conditions, the mass flow rate of the fluid through any transverse section of the medium $\dot{m}(z)$, is constant along the core length and is related to the flow rate by $\rho(z)q(z) = \dot{m}(z) = \dot{m}$, where $\rho(z)$ is the gas density.

For an ideal gas, $PV = nRT$, or $P = \rho RT/M_w$, where R is the ideal gas constant, T the absolute temperature, and M_w is the molecular weight of the gas. Combining Darcy's law from Eq. (2) with the continuity and ideal gas equations, the permeability at z is

$$\kappa(z) = -\frac{RT(z)\,\eta(z)\dot{m}}{M_w}\left(P(z)\frac{dP(z)}{dz}\right)^{-1}. \tag{3}$$

For an isothermal gas flow, the permeability $\kappa(z)$ is completely determined by the knowledge of the pressure $P(z)$, as the viscosity dependence on density is negligible [11].

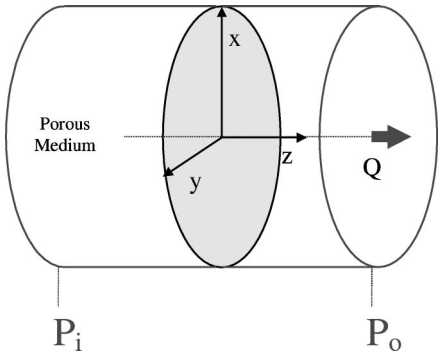

FIG. 1. Schematic diagram of the model.

*Correspondence and requests for materials should be sent to email address: bencsik@magres.nottingham.ac.uk

It is possible to obtain a three-dimensional mapping of $\underline{\kappa}(\mathbf{r})$ using this technique. However, only one projection of the local permeability tensor can be measured, that dictated by the local flow vector. If the local fluid flow vector at position $\mathbf{r}$ is along $\mathbf{s}$, $\mathbf{q}(\mathbf{r})=q(\mathbf{r})\mathbf{s}$, and if the direction of the local pressure gradient at $\mathbf{r}$ is along $\mathbf{u}$, $\nabla P(\mathbf{r}) = [\partial P(\mathbf{r})/\partial \mathbf{r}]\mathbf{u}$, then

$$\kappa_{su}(\mathbf{r}) = -q(\mathbf{r})\,\eta\left(\frac{\partial P(\mathbf{r})}{\partial \mathbf{r}}\right)^{-1}. \tag{4}$$

Mapping the three-dimensional fluid flow vector $\mathbf{q}(\mathbf{r})$ can be accomplished using q-space imaging techniques [12]. Microimaging studies of gas flow have recently been demonstrated by a number of groups [13,14]. Three-dimensional mapping of the pressure field can be performed with an appropriate 3D imaging sequence such as backprojection or single point imaging. Thus, a direct three-dimensional mapping of the permeability can be achieved.

The spatial resolution of the NMR imaging experiments can be an important factor, as these measurements are inherently discrete spatially, while Eqs. (3) and (4) above are continuous. If the pressure or flow distributions are heterogeneous within a single imaging voxel, the measured permeability is an effective permeability at the spatial resolution of the experiment.

METHODS

In practice the NMR signal in a gas has a complex dependence on density as it is weighted by the longitudinal and transverse relaxation times (T_1 and T_2 respectively) and the diffusion coefficient of the gas D, all of which also depend on density. It is usually not possible to make an NMR experiment short enough to ensure that these weighting factors are negligible. The NMR signal is therefore calibrated as a function of gas pressure in the absence of a pressure gradient, and it is assumed that this calibration remains valid in the presence of the pressure gradient.

As the signal to noise ratio (SNR) is generally low in gas-phase NMR experiments, it is essential to maximize it by adjusting the recycle time t_R with respect to T_1. However, T_1 depends on pressure, and is observed to be approximately proportional to it, $T_1=\beta P$, in the range of pressures investigated. For a fixed t_R and a 90° radiofrequency (RF) pulse, the calibration curve for signal strength S versus gas pressure P, is

$$S = \alpha P\left[1-\exp\left(-\frac{t_R}{\beta P}\right)\right], \tag{5}$$

where α is a constant that depends on the RF detection process and the number of spins per molecule of the gas, provided that the echo time t_E is short enough.

Note that care should be taken to ensure that molecular displacements (due to the pressure gradient) during the image acquisition are negligible compared with the spatial resolution of the imaging. Only permeabilities below a certain threshold can be measured, otherwise the fluid flow will be too rapid. A one-dimensional gradient echo sequence with a hard 90° pulse was used in the experiment. For the shortest echo times used ($\approx 400\ \mu$s), the upper limit for the permeability measurement was approximately 10 milliDarcy (mdarcy). This limit could be increased with faster gradient switching or the use of single point imaging or backprojection techniques.

The signal acquisition duration is limited by the hardware performance, while spatial resolution is primarily set by the acceptable SNR for the desired accuracy on κ. The technique is inapplicable in situations where the permeability of the medium is affected by the gas, as for example by adsorption in coals. Finally, the internal local magnetic field gradients in the porous medium should be as small as possible. Typically, T_2^* needs to be longer than 1 ms. An alternative approach is to use single point imaging techniques, where the signal acquisition time can be reduced to the order of 50 μs, which improves the signal to noise ratio and minimizes the displacement of gas molecules during the measurement.

The experiments were performed on a 2.35 T Bruker Biospec, horizontal bore system. Fluorine-19 NMR (95 MHz) measurements were performed using an inert, fluorine-rich probe gas, heptafluoropropane ($CF_3-CHF-CF_3$, HFA-227). A 90° RF excitation pulse was used, followed by a gradient-echo NMR experiment, with the gradient applied in the direction of the bulk gas transport, resulting in one-dimensional profiles.

The porous medium was first saturated with pure HFA-227. MR profiles of the gas-saturated medium were then obtained at various static pressures in order to calibrate local signal strength with pressure. A steady-state pressure gradient was applied to the system and another MR profile acquired. The map of fluid pressure in the flowing gas was then reconstructed using the calibration.

RESULTS

Experiments were performed on two samples with known bulk permeability of the order of 1 mdarcy: a sample of Indiana limestone, a commonly used building rock with spatially homogeneous permeability, and a North Sea oil reservoir sandstone, with clay particles interleaved between the silica grains. Gas adsorption was found to be negligible in both cases.

Figure 2(a) illustrates a 1D profile of the gas flowing in a cylindrical plug (25.4 mm in diameter, 61.5 mm in length) of Indiana limestone. The sample was placed in a nitrile sleeve experiencing an inward radial pressure of 15 bar to prevent by-pass flow around the cylinder. Indiana limestones exhibit low permeability, low susceptibility effects [15] (T_2^* of the order of 10 ms), and homogeneous features on length scales greater than 1 mm [1].

The echo time used was $t_E=560\ \mu$s and the recycle time was $t_R=70$ ms. Single shot signal acquisition lasts approximately 2 ms, during which the typical net displacement of a gas molecule is 12 μm which is negligible compared with the spatial resolution of 470 μm. The pressure calibration resulted in a value of $\beta=23.5\times10^{-3}$ s/atm, which was ob-

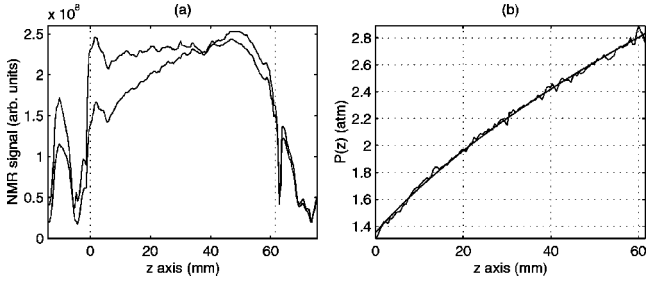

FIG. 2. Results in the building rock. (a) Gradient echo gas profiles in the Indiana limestone. The rock lies between the dotted lines. Signal outside the rock comes from gas in the fluid distributor plates and the nylon pipes used to deliver the gas. The upper (relatively flat) profile results from static gas saturating the stone at 2.4 atm. The lower (negative slope) profile is obtained from gas flowing from right to left. Inlet pressure=3 atm, flow rate at the outlet= 28.5 ml/min. Each profile is obtained from 23 000 acquisitions and takes 30 minutes to collect (t_R=70 ms, t_E=560 μs). (b) Gas pressure drop curve calculated from the flowing gas curve displayed in (a). The smooth continuous curve is a plot of the theoretical expression for a homogeneous stone [Eq. (6)]. The small deviations of the data from this curve are within the thermal noise of the measurement.

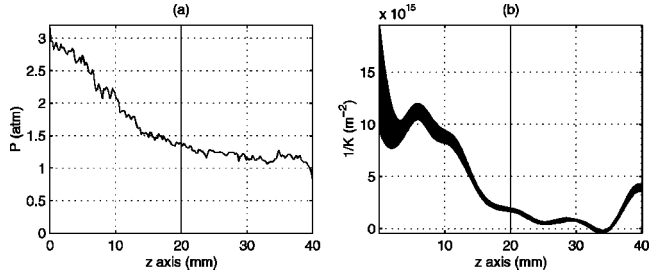

FIG. 3. Results in the two-stone system. (a). Gas pressure drop curve calculated from the gradient echo gas profiles for the two stacked stones. The sandstone lies between 0 and 20 mm. Most of the pressure drop occurs across this stone. The limestone is located between 20 and 40 mm. Profiles were acquired with 25 000 averages (t_R=127 ms, t_E=380 μs). (b) Spatial distribution of the reciprocal of the permeability, derived from the curve of (a). Line thickness is twice the standard error (due to thermal noise). At very high permeability, the data becomes unreliable, as the thermal noise is of the same order as the data. Spatial resolution is approximately 4 mm.

served to be approximately constant over the length of the stone.

Figure 2(b) shows the pressure drop obtained after numerical inversion of Eq. (5) for each pixel. There are nonnegligible pressure drops in the thin nylon tubing at the gas inlet and outlet of the sample. This explains why the inlet pressure is slightly lower than 3 atm and the outlet pressure is slightly higher than 1 atm. The figure also shows the best fit of the data to the theoretically expected pressure drop,

$$P(z)=\sqrt{\left(\frac{P_i^2-P_o^2}{L}\right)z+P_o^2}, \tag{6}$$

obtained from Eq. (3) for a medium with constant permeability, where P_i and P_o are the gas pressures at the inlet and outlet, and L is the length of the sample. The fit yields P_i =2.83 atm and P_o=1.35 atm. The excellent agreement between the two curves further validates the pressure measurement.

In the next experiment a shorter (length=20 mm) cylinder of Indiana limestone with bulk permeability 1.16 ± 0.02 mdarcy was stacked with an identical cylinder of North Sea sandstone exhibiting a bulk permeability 0.13 ± 0.02 mdarcy which is 8.8 ± 0.2 times lower than the limestone. The stones were placed in the same sample holder under identical conditions to the previous experiment and the gradient echo experiments performed with an echo time of 380 μs and a recycle time of 127 ms. Figure 3(a) shows the pressure drop across the two stones. This curve is convolved with a Gaussian smoothing function (standard deviation=2 mm), multiplied by its gradient and then normalized by its integral, which is proportional to the reciprocal of the known bulk permeability of the system. Figure 3(b) shows the spatial distribution of the reciprocal of the permeability. Validation of the method is provided by the estimate it gives of the ratio of the two stones bulk permeabilities. The integral of the curve in Fig. 3(b) is calculated between 0 and 20 mm and between 20 and 40 mm. The ratio of the integrals is 7.4 ± 0.6, and is independent of the above calibration procedure.

As the fluid enters and exits the stones, it probes a smaller surface area than the total one because of the narrow pipe transporting the gas into and out of the stones. Thus, it effectively experiences a lower permeability at the ends, a so-called ''end effect.'' If the data between 0 and 7 mm and between 33 and 40 mm is rejected, the predicted ratio of permeabilities turns out to be 7.7 ± 0.7. Thus, the result is not significantly biased by these ''end effects.'' The small discrepancy between the NMR result and the bulk permeability measurement could be due to the fact that water was used for the bulk permeability measurements, and the end effects are different for the two fluids. In addition, the gas used is not an ideal gas, and there could be small surface interactions between the gas and the pore surfaces affecting the validity of Eq. (3).

CONCLUSIONS

A direct method for measuring the spatial distribution of the hydraulic permeability of a porous medium has been presented here. It is both noninvasive and nondestructive, and uses the strong sensitivity of the NMR signal to the nuclear spin density. It may be possible to use the same principle with other noninvasive means of gas density measurement, such as Positron Emission Tomography. However, the superior temporal and spatial resolutions usually achieved with MRI makes it a more attractive choice.

The main application of the method is to improve single phase and multiphase fluid flow modeling in heterogeneous porous media. The method can provide measurements of the changes in the local permeability of a porous medium due to the presence of other fluid phases or solid particles, provided there is no interaction between the gas flow and the medium. Such interactions could involve bulk displacement of any

fluid already present or of loose solid particulates, or the dissolution of the probe gas in an existing liquid phase. The potential for noninvasive 3D mapping of the local permeability is unique to the method.

ACKNOWLEDGMENTS

M. Bencsik thanks Sir Peter Mansfield for his personal and financial support. We thank Dr. Martin Hürlimann (Schlumberger Doll research, Ridgefield, CT) and Dr. David Potter (Petroleum Engineering Department, Heriot-Watt University, Edinburgh, UK) for providing us with the Indiana limestone and with the North Sea oil reservoir samples (from the Pegasus project), respectively, and Professor Ken Packer (Department of Chemistry, University of Nottingham, UK) for providing us with the rock sample holder. We would like to thank Professor Packer and Professor Richard Bowtell (School of Physics and Astronomy, University of Nottingham, UK) for helpful discussions during the course of this work.

[1] R. W. Mair, G. P. Wong, D. Hoffmann, M. D. Hürlimann, S. Patz, L. M. Schwartz, and R. L. Walsworth, Phys. Rev. Lett. **83**, 3324 (1999).

[2] S. Torquato and M. Avellaneda, J. Chem. Phys. **95**, 6477 (1991).

[3] G. C. Borgia, V. Bortolotti, A. Brancolini, R. J. S. Brown and P. Fantazzini, Magn. Reson. Imaging **14**, 751 (1996).

[4] G. C. Borgia, R. J. S. Brown, and P. Fantazzini, J. Appl. Phys. **82**, 4197 (1997).

[5] K. J. Dunn, G. A. LaTorraca, and D. J. Bergman, Magn. Reson. Imaging **16**, 553 (1998).

[6] T. Friedmann and E. J. Windhab, Sep. Sci. Technol. **33**, 2221 (1998).

[7] K. J. Dunn, G. A. LaTorraca, and D. J. Bergman, Geophysics **64**, 470 (1999).

[8] M. Balzarini, A. Brancolini, and P. Gossenberg, Magn. Reson. Imaging **16**, 601 (1998).

[9] G. P. Frosch, J. E. Tilich, R. Haselmeier, M. Holz, and E. Althaus, Geothermics **29**, 671 (2000).

[10] J. Bear and Y. Bachmat, *Introduction to Modelling of Transport Phenomena in Porous Media* (Kluwer Academic, Dordrecht, 1990).

[11] For ideal gases, viscosity is actually independent of density. See, for example, S. Glasstone and D. Lewis, *Elements of Physical Chemistry* (MacMillan & Co. Ltd. London, 1960).

[12] P. T. Callaghan, *Principles of Nuclear Magnetic Resonance Microscopy* (Oxford University, Oxford, 1991).

[13] I. V. Koptyug, S. A. Altobelli, E. Fukushima, A. V. Matveev, and R. Z. Sagdeev, J. Magn. Reson. **147**, 36 (2000).

[14] G. Bennet and P. J. McDonald, *Proceedings of the 30th Congress Ampere on Magnetic Resonance and Related Phenomena* (Groupement Ampere, Lisbon, 2000).

[15] M. D. Hürlimann, J. Magn. Reson. **131**, 232 (1998).